Parameter Analysis on Longitudinal Lateral Force Resistance of Song Dynasty Timber Frame with Panjian

Yibin Chang,[a,b] and Jian Dai [a,b,*]

The Panjian structure is an important longitudinal connecting member of Song Dynasty hall-type buildings in China. To study the lateral force resistance of such structures, a refined finite element model of Song-style hall-type single-room four-column space timber frame containing Panjian structure was established based on the official building code *Yingzao Fashi* of Song Dynasty. The Panjian and inner E'fang in the lower-ping part, the Panjian in the upper-ping part, and Guazi-gong Panjian and Man-gong Panjian in the roof ridge part were investigated. The model hysteresis curves of all three parts of the longitudinal timber frame were found to be S-shaped, with obvious pinching effect, fuller at both ends and centrosymmetric shape. The Panjian structures in the lower-ping and upper-ping parts, and the Guazi-gong Panjian in the roof ridge part increased the energy dissipation and lateral stiffness of the timber frame. The Man-gong Panjian in the roof ridge part, however, was detrimental to the lateral resistance of the structure. Throughout the test, the Panjian structures were relatively intact, with large plastic damage occurring at both ends of the E'fang. For the repair and testing of similar ancient buildings, some reference suggestions are provided.

DOI: 10.15376/biores.18.2.2773-2788

Keywords: Traditional Chinese timber frame; Panjian; Lateral force resistance; Hysteretic behavior

*Contact information: a: Faculty of Architecture, Civil and Transportation Engineering, Beijing University of Technology, Beijing 100124, China; b: Key Science Research Base of Safety Assessment and Disaster Mitigation for Traditional Timber Structure (Beijing University of Technology), State Administration for Cultural Heritage, Beijing 100124, China; *Corresponding author: ibin1009@126.com*

INTRODUCTION

Traditional Chinese architecture is based on timber structures, which have evolved over the millennia and have developed a unique style in terms of architectural form and structural system. In the Northern Song Dynasty, the official architectural code *Yingzao Fashi* was issued, which made Chinese architecture enter a new stage of development and formed a new climax. The architectural structure is divided into the palace-type and the hall-type in the *Yingzao Fashi*. The palace-type timber frame is composed of the roof layer, Dou-gong layer, and column grid layer. The integrity of the Dou-gong layer makes the transverse structure and longitudinal structure have high similarity. The lack of a Dou-gong layer in the hall-type increases the difference between the structure in the transverse and longitudinal directions, thus increasing the difference in the lateral stiffness of the two directions. To maintain the integrity of the structure, the Panjian structure was set in the longitudinal direction of the building. The Panjian is a rectangular wooden bar, usually set under the purlins and connected at both ends to the Ling-gong, Guazi-gong, or Man-gong. This structure is mostly found in ancient buildings of the Tang and Song dynasties, as well as the Liao and Jin dynasties of the same period. However, the effectiveness of this setting

for improving the lateral stiffness of the structure is unknown. Therefore, it is necessary to study the longitudinal lateral force resistance performance of the Panjian structure on the Song-style typical hall-type buildings.

Many scholars have examined the lateral resistance of traditional timber frame structures. In China, Wang *et al.* (2021) investigated the influence of the Dou-gong layer, column head and column foot, load and position of vertical load on the hysteresis energy dissipation, and lateral force resistance of the palace-style timber frame in the Tang Dynasty. Shen *et al.* (2021) studied the force characteristics, hysteresis curve, skeleton curve, degradation of strength and stiffness, and energy dissipation law of the beam-raising timber frame of traditional residential houses in the northern region by means of a low circumferential reciprocal proposed static lateral resistance test. Chen *et al.* (2018) and Meng *et al.* (2019) conducted a proposed static test study on the Song-style single-room four-column timber frame model, revealing its seismic mechanism and the effect of loading history on its hysteretic energy dissipation and lateral stiffness resistance. Chen (2016) investigated the force performance of single-bay beam-raising and Chuan-dou timber frames of the Qing Dynasty based on theoretical analysis, finite element simulation and model test methods, respectively. In Japan, Kaori (2019) carried out shaker tests on four different types of bracket complexes. The results were compared with those obtained by static lateral loading tests, and the validity of a proposed structural model was discussed. Maeno *et al.* (2004) conducted a simulated static and shaking table test study on a Japanese four-column traditional building model and concluded that the restoring force of such timber frames is provided by the resisting moment of the crossbeams and the restoring force generated by the sway of the columns.

The above research results are focused on the transverse seismic performance or lateral resistance of traditional building structures, while less research has been conducted on the longitudinal lateral resistance of structures. Guo *et al.* (2021) designed a single-storey, two-span longitudinal timber frame and a transverse timber frame footprint model of the Chuan-dou type, and studied the seismic performance of the timber frame model through low circumferential reciprocal loading tests, and proposed a simplified bifold load-displacement model for longitudinal and transverse pierced bucket timber structures. The Panjian structure, an important component of the longitudinal structure, has been studied by a small number of researchers from the perspective of architectural form. Cao (2012) focused on the term Panjian from the three aspects of name, form, and meaning, and discussed the longitudinal components of timber structure. Jiang (2012) explained the nature of Panjian structure, usage rules, and development by sorting out and comparing the existing examples of Panjian forms.

In sum, the existing research results are based on the transverse lateral resistance of timber structures of traditional buildings, with little research on the longitudinal lateral resistance, and even less research on the longitudinal lateral resistance of typical Song-style official beam-raising buildings, especially on the mechanical properties of Panjian structures, with almost no results. Therefore, in order to study the mechanical role of Panjian structure in the timber frame, a refined model of the hall-type with Panjian structure was established according to the *Yingzao Fashi*, and its lateral force resistance mechanism was studied through horizontal simulations of proposed static loading, and the effects of Panjian structure at different parts in the building, such as lower-ping, upper-ping, and roof ridge, on the hysteretic energy dissipation and lateral force resistance of the timber frame were analyzed in depth.

EXPERIMENTAL

Construction of Song-style Hall-type Timber Frame with Panjian

As shown in Fig. 1, the studied hall is a typical Song-style hall-type wooden structure. Figure 2 shows a transverse section of the structure, with the timber frame being symmetrical in the transverse direction. In this profile, the parts along the longitudinal direction of the frame, from top to bottom, are named roof ridge part, upper-ping part, lower-ping part, and eaves part. The timber frame is transversely lapped by columns, beams and other components, with the outer row being the eaves columns and the inner row being the inner columns. The inner column is connected to the four-rafter beam by a Lu-dou. Two upper-ping Shu-columns are inserted on the four-rafter beam. The upper-ping Shu-columns are connected to the Ping-beam by means of the Jiaofu-dou. On the Ping-beam, the roof ridge Shu-column and other components are placed (Fig. 3).

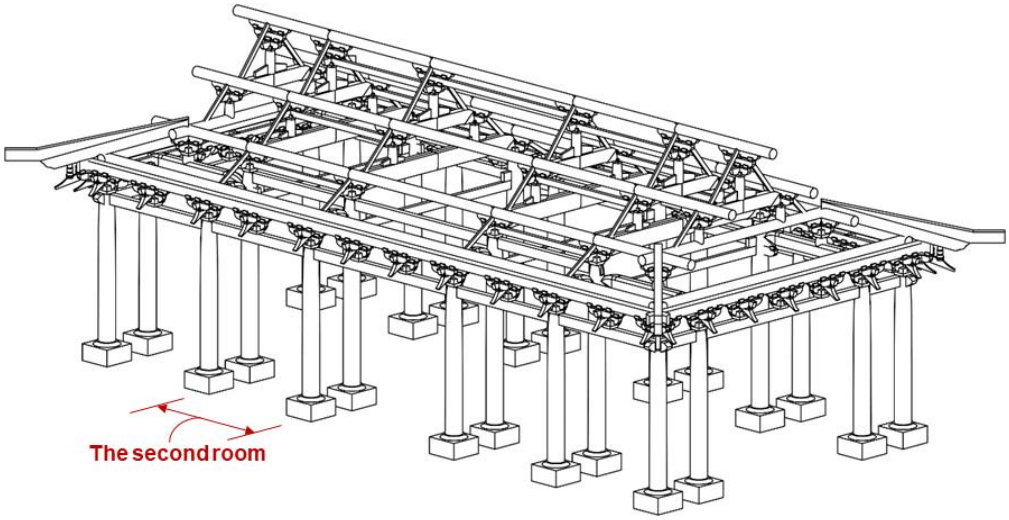

Fig. 1. The typical Song-style hall-type timber frame

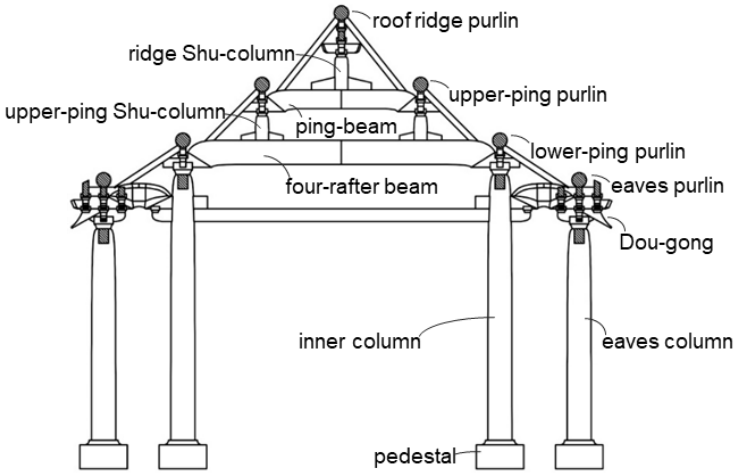

Fig. 2. Transverse section of the frame

For the longitudinal lower-ping part, the inner column is connected by inner E'fang, and the two ends of inner E'fang are made into dovetail. The Lu-dou is placed on the inner column, and they are connected by the column-head tenon. The Ling-gong is placed on the

Lu-dou. In order to increase the integrity of the structure, two adjacent Ling-gong are indirectly joined together and thus form a new element, the Ling-gong Panjian. The Qixin-dou is placed in the middle of the upper part of the original Ling-gong, and the San-dou is placed at both ends. The Ti-mu is placed on San-dou and Qixin-dou. The purlins of the two rooms are supported on Ti-mu, and the purlins are connected to the purlins by dovetail. Thus, in the position of lower-ping part, the connection of two product frames is realized by the above components. The longitudinal connection of the upper-ping part is almost the same as that of the lower-ping part, except that the inner E'fang is missing.

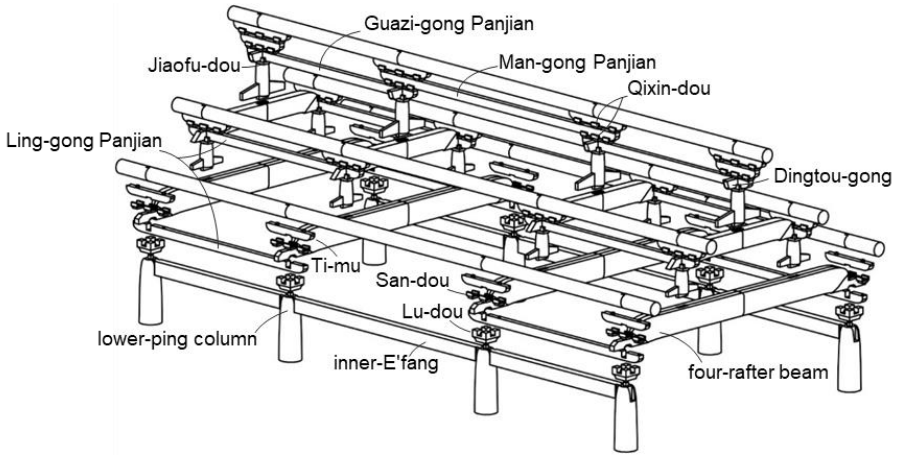

Fig. 3. The components and connections of the Panjian structures

The longitudinal structure of the roof ridge is slightly more complicated. If there is no Panjian structure, the ridge Shu-column is placed on the Jiaofu-dou, on which the Guazi-gong is placed. Two San-dou and a Qixin-dou are placed on the Guazi-gong and the Man-gong is placed on top of them. On the Man-gong are placed two more San-dou and a Qixin-dou, and on them are placed Ti-mu, on which the purlin of the two rooms are supported. If two Guazi-gong are connected, the new structure formed is the Guazi-gong Panjian, and if two Man-gong are connected, the new structure formed is the Man-gong Panjian. *Yingzao Fashi* stipulates that only one Panjian structure on the same level should be set up between adjacent rooms. This provision is due to the fact that the length of the wood is limited except for the roof ridge. However, at the roof ridge, the Guazi-gong and Man-gong are at different heights, and thus the Panjian structure can be set continuously.

Dimensions of Finite Element Model

The model of the hall-type timber frame was based on the *Yingzao Fashi*, with six rafters in the transverse direction and five rooms in the longitudinal direction (Fig. 1). The second room was selected as the object of finite element simulation. Three basic models were designed to simulate the lateral resistance of the timber frame at three locations, lower-ping, upper-ping and roof ridge, respectively, under seismic action. The finite element models of the timber frame are shown in Fig. 4. The dimensions of the components of the model are shown in Table 1. The proposed static test was carried out based on ABAQUS finite element software. The finite unit was an eight-node hexahedral linear unit. The members were connected by mortise and tenon. The action between the components was set by "contact", and the normal action was simulated by "hard contact"; the tangential friction was selected as Coulomb friction type. The friction coefficient was 0.4 (Xie *et al.* 2018).

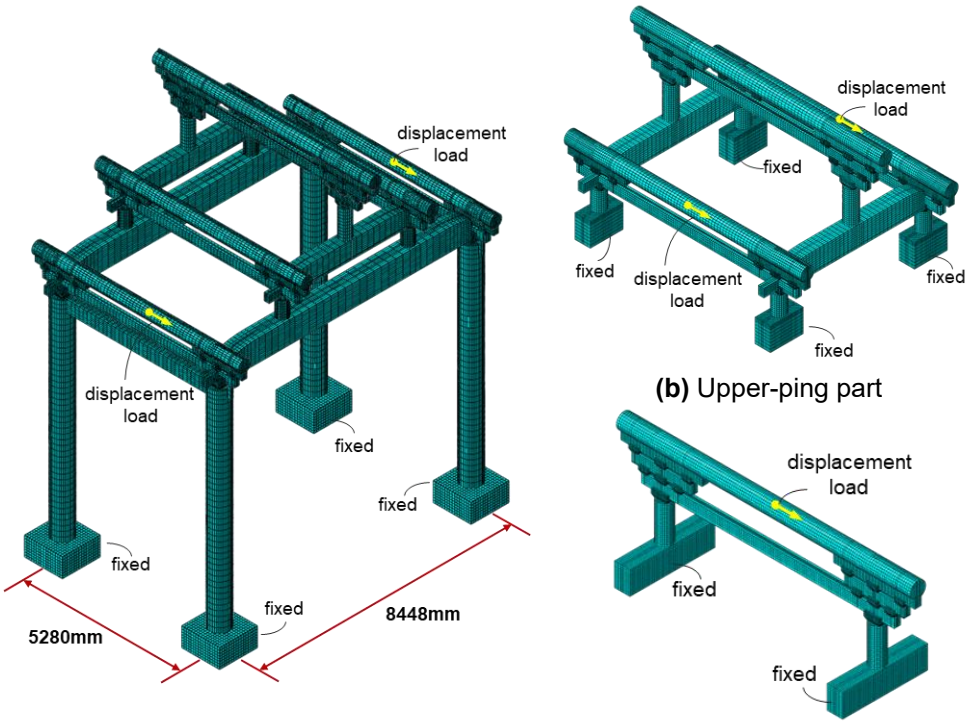

(a) Lower-ping part **(b)** Upper-ping part **(c)** Roof ridge part

Fig. 4. Refinement finite element model

Table 1. Dimensions of Components

Component Name	Width (mm)	Height (mm)	Length (mm)
Purlin	384	384	5280
Ti-mu	160	240	1664
Man-gong Panjian	160	240	7296
Guazi-gong Panjian	160	240	6272
Ling-gong Panjian	160	240	6432
San-dou	224	256	160
Qixin-dou	256	256	160
Jiaofu-dou	288	384	192
Lu-dou	512	512	320
Ridge Shu-column	360	360	640
Upper-ping Shu-column	360	360	880
Inner column	640	640	7056
Ping-beam	384	576	5277
four-rafter beam	480	720	9504
inner E'fang	256	384	5280
Pedestal	1267	1267	758

Material Parameters

In finite element software simulations, wood is modelled using an orthogonal anisotropic intrinsic model. The wood selected for this study was camphor pine (Li 2015), and its mechanical properties parameters are shown in Table 2. The pedestal was made of granite with a modulus of elasticity of 55000 MPa, Poisson's ratio of 0.2, and a density of 2800 kg/m^3.

Table 2. Material Property Parameters of Camphor Pine

Elastic Modulus (MPa)			Poisson's Ratio			Shear Modulus (MPa)			Density kg/m^3)
E_L	E_R	E_T	U_{RL}	U_{TL}	U_{TR}	G_{LR}	G_{RT}	G_{LT}	ρ
3805	268	154	0.5	0.1	0.35	268	154	268	460
Note: *E* is the elastic modulus; *U* is Poisson's ratio; *G* is the shear modulus; L, R, and T refer to the longitudinal, radial, and tangential directions respectively; *ρ is* the density.									

Roofing Load

In accordance with the official traditional timber roof construction practice (Liu 2001a,b), the roof layers from top to bottom are the barrel-tiles, gray lime-back, white lime-back, straw clay-back, board-guard lime, wang-board, and rafters. In Table 3, the weight of each layer of material for the roof was counted. An equivalent surface load of 7.12 kN/m^2 was calculated for the roof covering. From this, the line loads on the lower-ping purlin, upper-ping purlin and roof ridge purlin were 17.58, 19.29, and 20.23 kN/m respectively.

Table 3. Calculation of Roof Load

Layered Construction	Thickness (cm)	Mass (kg/m^2)	Weight (kN/m^2)
Barrel-tiles	-	264	2.59
Gray lime-back	3	51	0.50
White lime-back	3	51	0.50
Straw clay-back	8	160	1.57
Board-guard lime	1.5	32	0.31
Rafter with Wang-board		133	1.30
Snow load			0.35
Grand total			7.12

Loading Scheme

In order to investigate the effect of the Panjian structure on the lateral resistance of timber frames at three locations, the lower-ping, the upper-ping, and the roof ridge, three basic models were designed (Fig. 4). For each basic model, horizontal low circumferential cyclic displacement load were applied to the middle of the purlins. In the lower-ping model, the pedestal was fixed (Fig. 4a). The load displacement was increased in steps of ±50 mm, and the maximum magnitude was ±500 mm, for a total of 10 cycles. In the upper-ping model, the four-rafter beam was fixed (Fig. 4b). The load displacement was increased in steps of ±20 mm, and the maximum magnitude was ±200 mm, for a total of 10 cycles. In the roof ridge model, the Ping-beam was fixed (Fig. 4c). The load displacement was increased in steps of ±30 mm, and the maximum magnitude was ±300 mm, for a total of 10 cycles (Fig. 5).

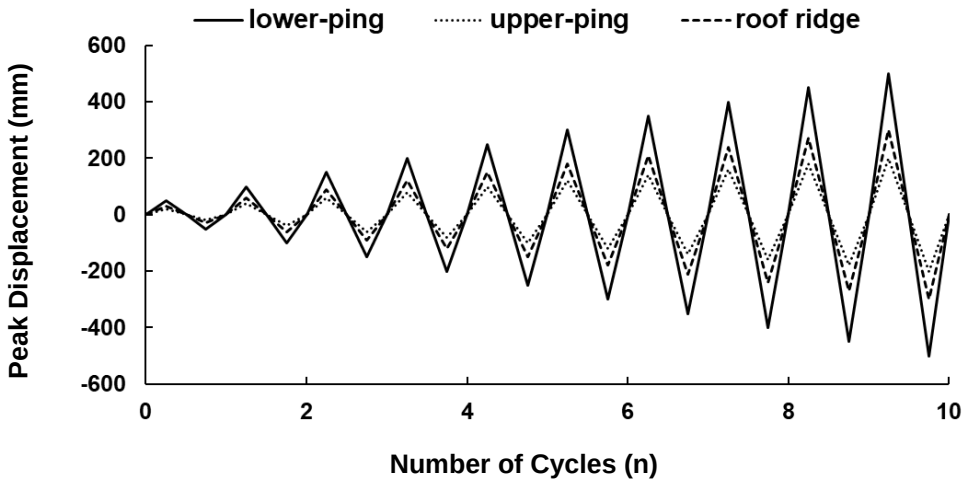

Fig. 5. Loading process of the test

RESULTS AND DISCUSSION

Lower-ping Part

In the lower-ping part, three models were designed in order to investigate the effect of the Panjian and inner E'fang on the lateral resistance of the timber frame. The model containing Panjian and inner E'fang was named LPPJ-1, the model without Panjian was named LPPJ-2, and the model without inner E'fang was named LPPJ-3.

Deformation characteristics

For the LPPJ-1, the timber structure swayed left and right under horizontal reciprocal loading and tilted toward the loading direction, and the structure above four-rafter beam remained almost horizontal and did not tilt and sway. The Panjian moved to the right with the horizontal load, the middle section was always straight, the left side bended upward less, while the right side bended and deformed more at the intersection with four-rafter beam. The Jiaofu-dou also tilted to the right, the right side of the top surface of Jiaofu-dou separated from Ti-mu, and the top surface of the rightmost San-dou had separated from Ti-mu. The Lu-dou on the column head moved horizontally with the swing of the column head. The bottom of Lu-dou on the left side of the column head fitted more tightly with the column head. The left side of the bottom of the Lu-dou on the right side of the column head was extruded and deformed from the column head. The right-hand bottom of the Lu-dou separated from the head of the column, thus creating a squeeze on the right-hand upper face and the lower left-hand lower face of the column-head tenon. The inner E'fang moved horizontally as the upper part of inner column swayed and tilted, and then it rotated relative to the inner column. The two ends of the inner E'fang were dovetail, and the upper left side and lower right side of its vertical end face were extruded from the mortise of inner column, and the rest of the large area was separated. The top surface of both ends of dovetail was extruded from the bottom surface of two Lu-dou, and the bottom surface of the right column-head tenon was extruded and deformed from the bottom surface of mortise. The two column legs were loaded to the right with the load, the left side was gradually lifted and separated from the pedestal, and the right side was extruded from the

pedestal. The bottom surface of column-foot tenon was separated from the top surface of mortise of the pedestal, and the left surface was extruded and deformed from the pedestal. The base of both columns gradually lifted up and separated from the pedestal on the left side as the load was loaded to the right, and it squeezed against the pedestal on the right side. The bottom face of the column-foot tenon was separated from the top face of the mortise of the pedestal, while the left face was extruded and deformed from the pedestal.

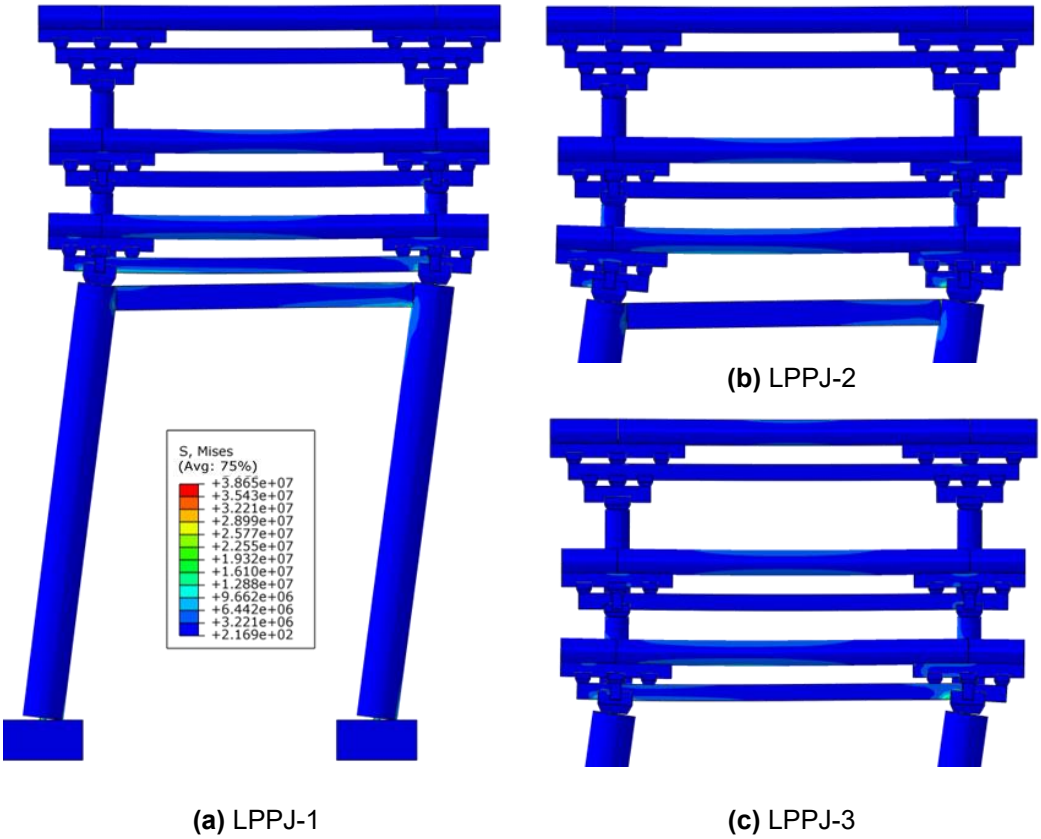

(a) LPPJ-1

(b) LPPJ-2

(c) LPPJ-3

Fig. 6. Deformation and stress diagram of timber frame

Figure 6a shows the stresses clouds of the LPPJ-1 at a forward loading of 500 mm. The Panjian was within the elastic range of the material throughout the reciprocal loading process, although large deformations were generated at both ends. In the reciprocal loading of the Lu-dou under horizontal load, the contact surfaces with the column-head tenon on both sides extruded each other. Due to the small radial modulus of elasticity of the column-head tenon, it partially deformed but did not enter plasticity. The inner E'fang, under horizontal loading, mainly rubbed against the bottom surface of the Lu-dou and the bottom surface of the mortise side of the inner column. These extrusion deformations occurred mostly in the radial direction of the inner E'fang, and as the radial modulus of elasticity was less than the longitudinal direction, the member developed a plastic strain due to excessive deformation. The column-foot tenon, like the column-head tenon, was radially compressed. As the modulus of elasticity of the granite was much greater than that of the timber, the column-foot tenon had a large area of plastic deformation.

For LPPJ-2 and LPPJ-3, the overall deformation under horizontal reciprocating loads was similar to that of LPPJ-1(Fig. 6b and Fig. 6c). In LPPJ-2, there was a clear

separation between the San-dou and Ti-mu on the Ling-gong. This reduced the integrity of the member between the Lu-dou and lower-ping purlin, which in turn affected the lateral resistance. In LPPJ-3, the inner E'fang was missing to resist lateral displacement, and the frictional dissipation of the inner E'fang and inner column disappeared.

Hysteresis curve

The load-displacement hysteresis curve of a structure can reflect its energy dissipation capacity, structural damage form, load carrying capacity, stiffness and strength degradation under repeated loading, which is a comprehensive evaluation method and basis for seismic performance.

Figure 7 shows the lower-ping part with the hysteresis curves for the three models. For the LPPJ-1, the hysteresis curve is S-shaped. The course is centrally symmetric and has a very pronounced pinching effect. This indicated that large frictional slip and extrusion deformation occurred between Lu-dou, inner E'fang, and inner column. Such slip and deformation also occurred between the Panjian structure and between column-foot tenon and mortise of the pedestal during the loading process. The hysteresis curves were full at both ends, indicating that the structure experienced strong hysteresis dissipation in the middle and late stages of loading. When the load was unloaded to 0, the displacement angle corresponding to the maximum residual displacement was only 0.16%, indicating that the LPPJ-1 had good recovery ability after large deformation. At the early stage of loading, when $\Delta < 50$ mm, the hysteresis curve developed roughly linearly, and the hysteresis loop was small. At this time, because the loading displacement was very small, there was no large deformation between the wood members, and the material was still in the elastic stage. When $\Delta \geqslant 50$ mm, the hysteresis curve began to develop nonlinearly, the hysteresis curve area increased, and the pinching phenomenon appeared. The mutual friction and extrusion deformation between the components was increasing, and the energy consumption also started to increase.

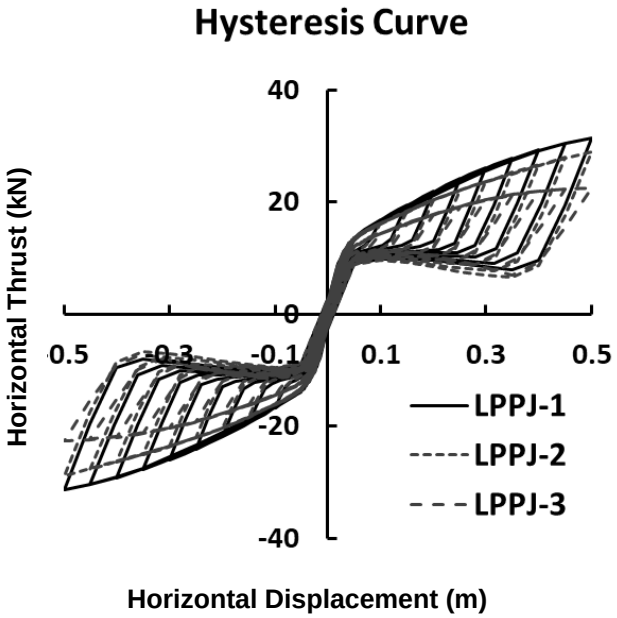

Fig. 7. The load-displacement hysteresis curves of the three models in the lower-ping part

The shape of the hysteresis curve of LPPJ-2 was similar to that of LPPJ-1, but the overall area was reduced by 2%. Compared to LPPJ-1, the hysteresis curve of LPPJ-3 was flatter at the ends and its overall area was reduced by an even greater 34%. This showed that the presence of inner E'fang had a greater effect on energy dissipation, while the Panjian structure had less effect on it.

Skeleton curve

The skeleton curve is the envelope formed by the first cycle peak point of each loading phase of the frame model under cyclic loading, which can reflect the lateral resistance of the frame model in different phases (Fig. 8). The skeleton curve of the LPPJ-1 was centrosymmetric. At the initial stage of loading, the rotational stiffness was larger, and the skeleton curve was steeper. When loaded to around 25 mm, the skeleton curve yielded. When loaded between 50 and 300 mm, the skeleton curve grew in a roughly diagonal straight line. The lateral stiffness slowly decreased and the horizontal reaction force continued to increase. At this stage, the members such as the capital and inter-loop on the head were more integral, the pipe leg tenons were extruded from the column base, and the members were mostly in the elastic phase. When the load displacement exceeded 300 mm, the skeleton curve grew slowly and the displacement increased sharply. This was due to the significant plasticity in the upper and lower tenons of the inner column and the ends of the inner E'fang, as well as the severe tilting of the structure, where the second-order distance of the vertical load increased and a smaller horizontal force could cause a larger horizontal displacement.

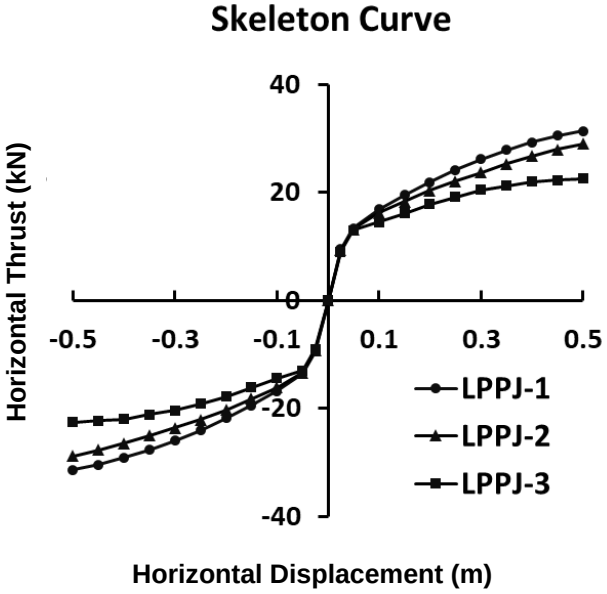

Fig. 8. The load-displacement skeleton curves of the three models in the lower-ping part

The skeleton curve trends for LPPJ-2 and LPPJ-3 were similar to those of LPPJ-1. Both skeleton curves yielded when loaded to near 25 mm. As the displacement increased, LPPJ-2 decreased by about 7% overall, while LPPJ-3 decreased by about 21%. This suggested that the inner E'fang and Panjian structures contributed to the lateral stiffness of the structure, but the contribution of the inner E'fang was greater than that of the Panjian structure.

Stiffness degradation

Under the action of horizontal low circumferential repeated load, the lateral stiffness of the structure resistance decreases with the increase of horizontal displacement and produces stiffness degradation. Structural lateral stiffness resistance is expressed by cut-line stiffness and calculated according to Eq. 1.

$$K_i = \frac{|+P_i| + |-P_i|}{|+\Delta_i| + |-\Delta_i|} \quad (1)$$

In Eq. 1, i is the number of loading cycles; K_i is the lateral stiffness of the timber frame at the i-th cycle; P_i is the peak load at the i-*th* cycle; and Δ_i is the peak displacement corresponding to P_i. From Fig. 9, the initial lateral stiffness of the three models was the largest and it decreased continuously with the increase of horizontal displacement. When $\Delta \leqslant 150$ mm, the degradation rate of lateral stiffness resistance was faster, and then it gradually tended to slow down. The initial stiffnesses of LPPJ-2 and LPPJ-3 decreased by about 2% and 5%, respectively, compared to LPPJ-1. As the displacement increased, the reduction in LPPJ-2 became 8%, while LPPJ-3 gradually decreased to around 23%, indicating that inner E'fang was more beneficial than Panjian in reducing the stiffness degradation of the structure.

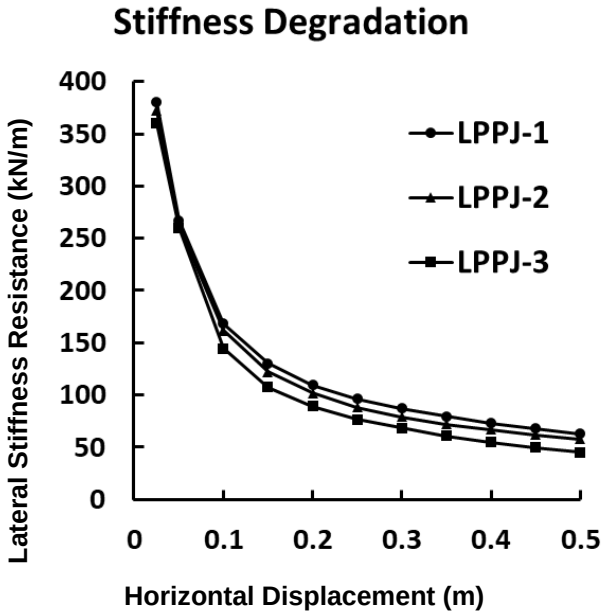

Fig. 9. The stiffness degradation curves of the three models in the lower-ping part

The above experimental phenomena showed that Panjian and inner E'fang could improve the longitudinal lateral stiffness of timber frames, with inner E'fang contributing more than Panjian structure. This was due to the large size of the inner E'fang, which was connected to the inner column at both ends by means of dovetails. When a reciprocating horizontal load was applied to the model, its ends effectively connected to the inner column and as the displacement increased, the dovetails rubbed against each other, squeezed and deformed plastically, thus increasing the energy dissipation.

Upper-ping Part

In the upper-ping part, two models were designed in order to investigate the effect of the Panjian on the lateral resistance of the timber frame. The model containing Panjian structure was named UPPJ-1, and the model lacking the Panjian structure was named UPPJ-2.

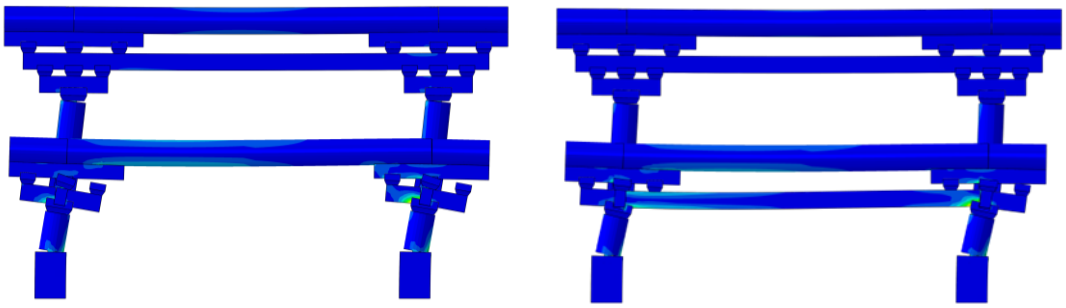

(a) UPPJ-1 **(b)** UPPJ-2

Fig. 10. Deformation and stress diagram of timber frame in the upper-ping part

Figure 10 shows the deformation diagram and stress diagram of the timber frame of UPPJ-1 and UPPJ-2 when the displacement was loaded to 250 mm. In UPPJ-1, the Jiaofu-dou was extruded and rubbed against the superstructure, and the San-dou on the right-hand Panjian separated slightly from the Ti-mu. The integrity of the Jiaofu-dou, Panjian, and superstructure was strong. In UPPJ-2, a significant separation of the San-dou from the Ti-mu occurred at both ends. This reduced the integrity of the upper members of the Jiaofu-dou. Compared to UPPJ-1, the interaction between the UPPJ-2 members changed from squeezing and friction between the Jiaofu-dou and four-rafter beam ends and Panjian to squeezing and separation of the sandou and Ti-mu.

Figure 11 shows the hysteresis curves for the upper-ping structure. The shape of the hysteresis curve of the upper-ping Panjian frame was somewhat different from that of the lower-ping Panjian frame.

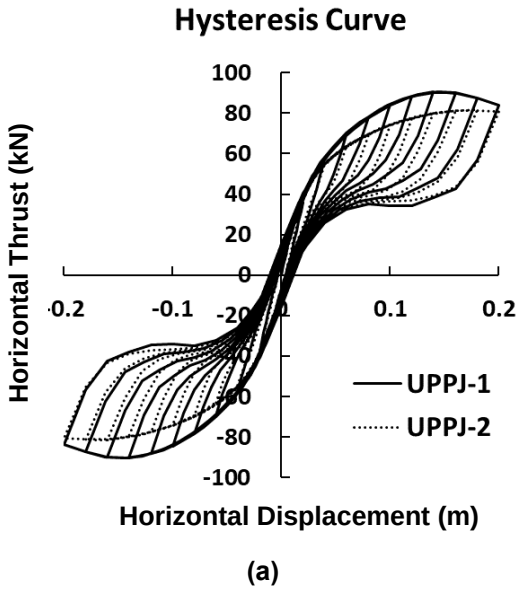

(a)

Fig. 11 (a). Hysteresis curves, skeleton curves and stiffness degradation curves of the two models in the upper-ping part

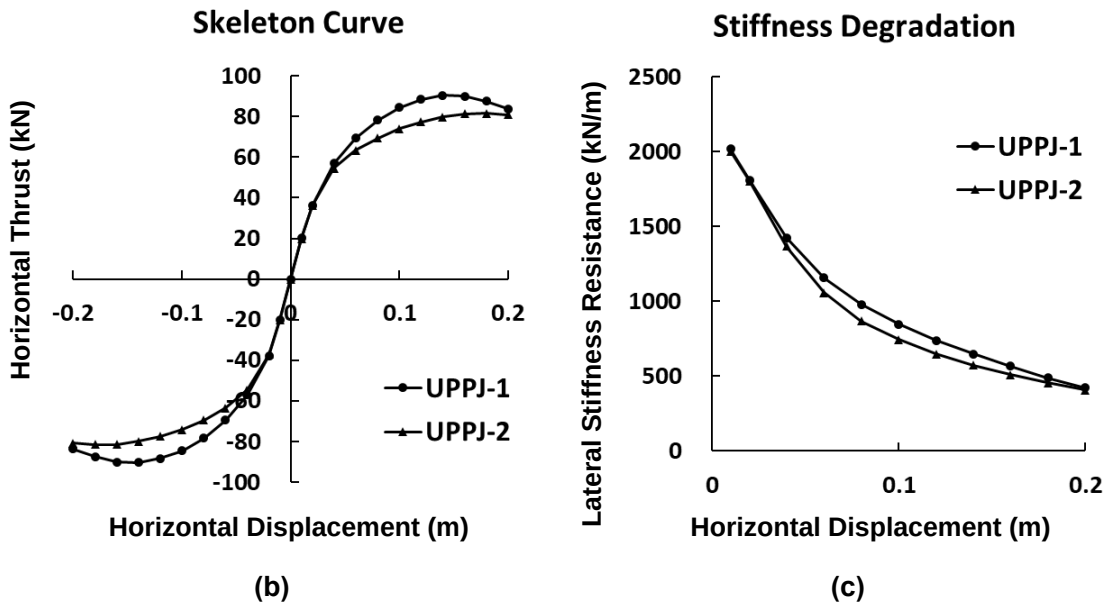

Fig. 11 (b & c). Hysteresis curves, skeleton curves and stiffness degradation curves of the two models in the upper-ping part

This was mainly due to the absence of the inner E'fang, which was an important structure in the upper-ping frame compared to the lower-ping frame. The second was the change from the long, thick inner column to the short, thin Shu-column, and the difference in the size of the tenons at the base of the two columns.

With Fig. 11, the area of the hysteresis curve for model UPPJ-2 was reduced by approximately 14% compared to model UPPJ-1. The lateral stiffness was reduced by an average of 6% throughout the displacement loading process. This indicated that the Panjian structure played a role in the lateral resistance performance of the model as well as the hysteresis energy dissipation.

Roof Ridge Part

Three models were formed by the presence or absence of Panjian structures at the roof position. They were the Guazi-gong Panjian model named GZPJ, the Man-gong Panjian model named MGPJ, and the model lacking Panjian named RLPJ. Here RLPJ was used as the basic model.

Figure 12 shows the hysteresis curves of the three models. Compared with model RLPJ, the hysteresis area of MGPJ increased by 1%, while the hysteresis curve area of GZPJ decreased by 2%, indicating that the Man-gong Panjian structure does not improve the hysteresis energy dissipation of the structure.

In the skeleton curves, compared with model RLPJ, the lateral stiffness of MGPJ decreased by 3% and the lateral stiffness of GZPJ increased by about 8%, indicating that Guazi-gong Panjian improves the lateral stiffness of the structure, while Man-gong Panjian decreased the lateral stiffness of the structure instead. In the stiffness degradation curves, the stiffness of the MGPJ and GZPJ increased by 3% and 16% respectively compared to the RLPJ model.

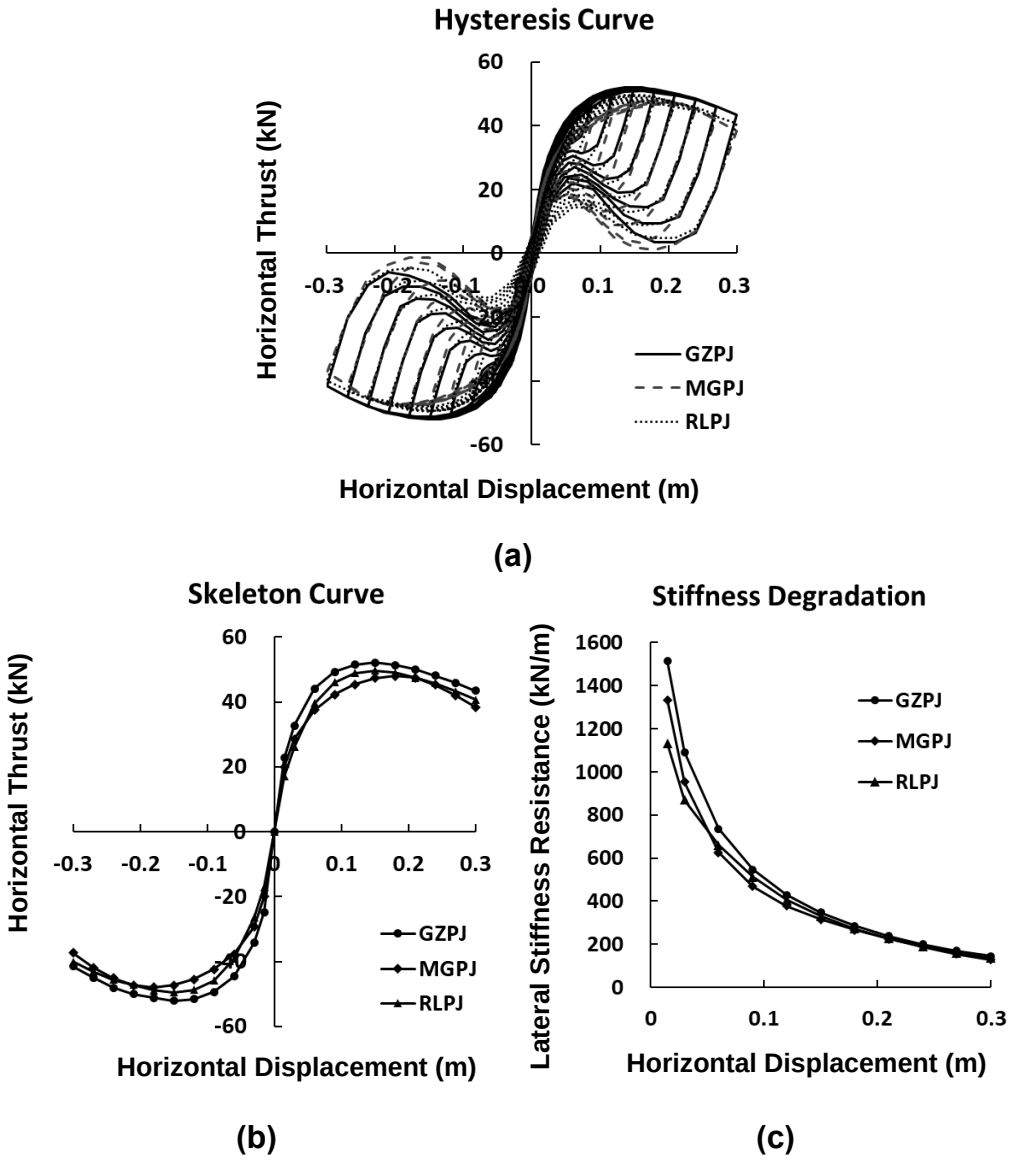

Fig. 12. Hysteresis curves, skeleton curves and stiffness degradation curves of the three models in the roof ridge part

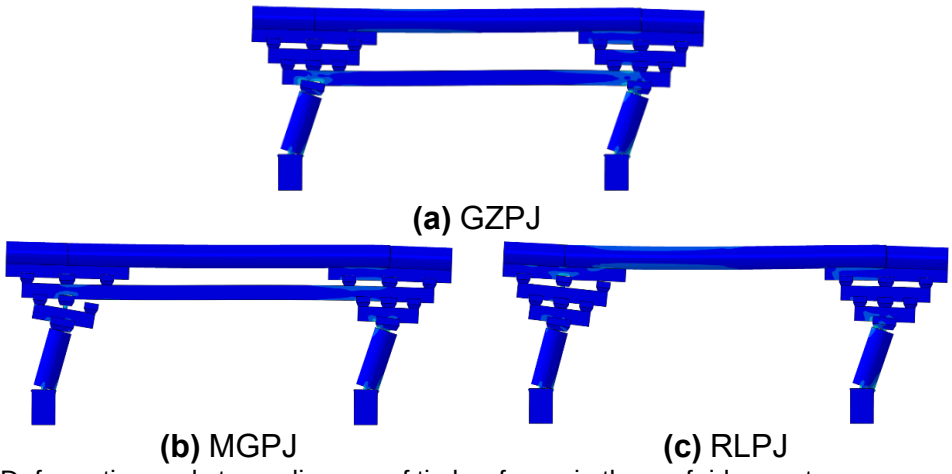

Fig. 13. Deformation and stress diagram of timber frame in the roof ridge part

The hysteretic energy dissipation and lateral stiffness resistance of Guazi-gong model were greater than the other two. With Fig. 13, the causes of the deformation were analysed in relation to the deformation characteristics of the three models. Due to the presence of Guazi-gong Panjian, the upper part of the structure maintained a strong integrity. Under reciprocating horizontal loads, friction and extrusion occurred between Panjian, Shu-columns, and Jiaofu-dou. Especially in the later stages of loading, the Shu-columns showed large areas of plasticity. These increased the energy dissipation of the GZPJ. Although the Panjian was present in the MGPJ, the structural integrity below the Man-gong was relatively loose. The San-dou and Qixin-dou on the Man-gong appeared to separate from the Panjian during the left-right reciprocal horizontal load loading. This caused a part of the members to appear open and closed, reducing the energy dissipation from extrusion friction. Compared to the MGPJ model, the RLPJ model lacked the Panjian connection, but the left and right parts of the upper part of the Shu-column were more intact during loading, thus causing the hysteretic energy dissipation and lateral stiffness to be greater than that of the MGPJ model.

CONCLUSIONS

1. The modeled hysteresis curves of Song-style longitudinal timber frame at the three locations of the lower-ping, the upper-ping and the roof ridge were S-shaped, with an obvious pinch shrinkage effect. The ends were fuller and the shape was centrally symmetrical.
2. In the lower-ping and upper-ping timber frames, the presence of the Panjian enhanced the integrity of the timber frame, increased the compression and friction between the members, and improved the hysteretic energy and lateral resistance of the frame. In the lower-ping part, the inner E'fang outperformed the Panjian element in terms of energy consumption and lateral force resistance. The ends of the inner E'fang showed large plastic damage. In the conservation of traditional ancient buildings, similar elements require focused attention.
3. In the timber frame at the ridge, compared to the Man-gong Panjian model and the model without Panjian, the Guazi-gong Panjian enhanced the integrity of the structure above the Jiaofu-dou, which in turn had the highest hysteretic energy dissipation and the highest lateral resistance. Although the Man-gong Panjian model added a Panjian structure, it weakened the integrity of the lower part of the Panjian structure, leading to a reduction in energy dissipation and lateral stiffness by 2% and 3% respectively. This indicated that the Guazi-gong Panjian, which was provided at the ridge, was beneficial for the lateral resistance of the timber frame, but the Man-gong Panjian was not.

ACKNOWLEDGMENTS

The study was supported by the National Natural Science Foundation of China (51678005).

REFERENCES CITED

Cao, X. (2012). *A Study on the Chinese Architecture Terminology "Panjian"*, Master's Thesis, Tianjin University, Tianjin, China.

Chen, C. C. (2016). *Integral Mechanics Property Analysis and Safety Evaluation of Ancient Timber Structures*, Ph.D. Dissertation, Southeast University, Nanjing, China.

Chen, J. Y., Li, T. Y., Yang, Q. S., Shi, X, W., and Zhao, Y. X. (2018). "Degradation laws of hysteretic behavior for historical timber buildings based on pseudo-static tests," *Engineering Structures* 156, 480-489. DOI: 10.1016/j.engstruct.2017.11.054

Guo, T., Yang, N., Zhou, H. B., and Wang, S. Y. (2021). "Experimental study of the seismic performance of Chuan-Dou-style longitudinal wooden frames," *China Civil Engineering Journal* 54(S1), 34-41. DOI: 10.15951/j.tmgcxb.2021.s1.014

Jiang, Z. (2012). "On the pattern and tectonic thinking of Pan-jian timber used in the wooden structures of Tang and Song Dynasty," *History of Architecture* 01, 83-92.

Kaori, F. (2019). "Dynamic performance of bracket complexes used in traditional timber structures in Japan," *Proceedings of the Japan Academy, Series B* 95(9), 568-580. DOI: 10.2183/pjab.95.038

Li, Y. Z. (2015). *Experimental Study on Seismic Behavior of Dovetail Mortise-tenon Joints under Different Loose Degrees in Ancient Timber Buildings*, Master's Thesis, Xi'an University of Architecture and Technology, Xi'an, China.

Liu, D. K. (2001a). "Load assembler of roofing of ancient building (The first volume)," *Traditional Chinese Architecture and Gardens* 3, 58-64.

Liu, D. K. (2001b). "Load assembler of roofing of ancient building (The second volume)," *Traditional Chinese Architecture and Gardens* 4, 56-63.

Maeno, M., Suzuki, Y., Ohshita, T., and Kitahara, O. (2004). "Seismic response characteristic of traditional wooden frame by full-scale dynamic and static tests," in: *13th World Conference on Earthquake Engineering*, Vancouver, B.C., Canada. No. 1184.

Meng, X. J., Li, T. Y., and Yang, Q. S. (2019). "Experimental study on the seismic mechanism of a full-scale traditional Chinese timber structure," *Engineering Structures* 180, 484-493 DOI: 10.1016/j.engstruct.2018.11.055

Shen, Y. L., L, H., Zhou, J. X., Chen, Z. W., Wang, L. H., and Zhou, H. B. (2021). "Experimental study on lateral performance of post-and-linteltimber frame in traditional residences," *Beijing University of Technology* 47(07), 759-772. DOI: 10.11936/bjutxb2021030007

Wang, J., Xu, R. W., Zhang, X. M., and Yang, Q. S. (2021). "Parameter analysis on lateral force resistance of the palace-style timber structure in Tang Dynasty," *Journal of Civil and Environmental Engineering* 44(02), 48-59. DOI: 10.11835/j.issn.2096-6717.2021.020

Xie, Q. F., Zhang, L. P., Xiang, W., and Qian, C. Y. (2018). "Experimental study and finite element analysis of Dou Gong joints built with fork column under vertical loading," *Journal of Building Structures* 39(9), 66-74. DOI: 10.14006/j.jzjgxb.2018.09.008

Article submitted: December 24, 2022; Peer review completed: January 14, 2023; Revised version received and accepted: February 12, 2023; Published: February 21, 2023.
DOI: 10.15376/biores.18.2.2773-2788